Strongly Interacting Spinors in One-Dimensional Harmonic Trap

I. GENERAL FORMULATION

First we will consider two strongly-interacting, ultracold bosons with a spin degree of freedom confined in a one-dimensional harmonic trap. For now, we assume that the interaction is a spin-independent point interaction. The Hamiltonian is given by

$$H = \sum_{i=1}^{N} \left[-\frac{1}{2}\frac{\partial^2}{\partial x^2} + \frac{1}{2}x_i^2 \right] + g \sum_{i<j} \delta(x_i - x_j) \tag{1}$$

where N is the number of particles, the constant g is the interaction strength, and we have set $\hbar = m = \omega = 1$. For spinless bosons, the many-body wave function can be found using the Bose-Fermi mapping [2] in the case of $g \to \infty$.

For the case of spinful particles, Yang et al. [5] obtain a second-order, effective Hamiltonian, which is written as

$$H_{\text{eff}} = -\frac{1}{g} \sum_{i=1}^{N-1} C_i (1 \pm \mathcal{E}_{i,i+1}) \tag{2}$$

where $\mathcal{E}_{i,i+1}$ is the exchange operator that exchanges the i^{th} particle with the $(i+1)^{th}$ particle. Plus is for bosons and minus is for fermions. Each C_i is a constant

$$C_i = N \int \prod_j dx_j \left| \frac{\partial \varphi_A}{\partial x_i} \right|^2 \delta(x_{i+1} - x_i) \theta^1_{[i+1,i]} \tag{3}$$

where φ_F is the slater determinant for our system of particles, and $\theta^1_{[i+1,i]}$ is the reduced sector function given by

$$\theta^1_{[i+1,i]} = \theta^1 / \theta(x_{i+1} - x_i) = \frac{\theta(x_2 - x_1) \cdots \theta(x_N - x_{N-1})}{\theta(x_{i+1} - x_i)}$$

Additionally, Yang et al. show that the one-body density matrix for these spinors can be separated into its spatial and spin components

$$\rho_{\sigma,\sigma'}(x, x') = \sum_{m,n} \rho_{m,n}(x, x') S_{m,n}(\sigma, \sigma') \tag{4}$$

where the spatial component

$$\rho_{m,n}(x', x) = (\pm 1)^{m-n} (N-1)! \int dx_2 \cdots dx_N \varphi_A^* \varphi'_A \theta^{(1,\ldots,m)} \theta'^{(1,\ldots,n)} \tag{5}$$

is just the one-body density matrix for the sector $x_2 < x_3 < \cdots < x_m < x' \cdots x_n < x \cdots < x_N$ for $m < n$. If the particles are bosons, the $\pm$ is a minus and if fermions it is a plus. The function $\theta^{(1,\ldots,n)}$ refers to a cyclic shift backwards for the first n indices of the sector function θ^1, i.e.,

$$\theta^{(1,\ldots,n)}(x, x_2, \ldots, x_N) = \theta^1(x_2, x_3, \ldots, x_n, x, \ldots, x_N)$$

More generally, the expression $(1, \ldots, n)$ denotes a cyclic permutation on the first n indices

$$x_1, x_2, \ldots, x_N \longrightarrow x_2, x_3, \ldots, x_n, x_1, x_{n+1}, \ldots, x_N$$

And the spin component of the one-body density matrix is

$$S_{m,n}(\sigma, \sigma') = [(1, \ldots, m) c_m(\sigma) |\chi\rangle]^\dagger [(1, \ldots, n) c_n(\sigma') |\chi\rangle] \tag{6}$$

where $c_m(\sigma')$ is a destruction operator for the m^{th} particle with spin σ'. For instance, $c_2(\frac{1}{2})$ destroys the second particle if it has spin $\frac{1}{2}$. If it does not, then $c_2(\frac{1}{2}) |\chi\rangle = 0$.

II. TWO SPIN 1/2 BOSONS

For the case of two spin-$\frac{1}{2}$ bosons, we can see that the eigenstates of the effective hamiltonian in equation (2) are just the states $|\chi\rangle$ that are symmetric under particle exchange. These eigenstates are easy to find because they correspond to the four total spin states for two spin-$\frac{1}{2}$ particles.

We will first consider the case where we have two strongly-interacting bosons with total spin state $|\chi\rangle = |S=1, M=1\rangle = |\uparrow,\uparrow\rangle$. First we calculate the spin component. It is immediately apparent that $c_m(\sigma')\,|\chi\rangle$ will be zero unless $\sigma' = \uparrow$, because that is the spin of both particles. It can be shown that for any $m, n \in \{1, 2\}$

$$S_{m,n}(\sigma, \sigma') = \begin{cases} 1 & \sigma' = \sigma = \uparrow \\ 0 & \text{else} \end{cases} \tag{7}$$

and thus our one-body density matrix is

$$\rho_{\uparrow,\uparrow}(x, x') = \rho_{1,1}(x, x') + \rho_{1,2}(x, x') + \rho_{2,1}(x, x') + \rho_{2,2}(x, x') \tag{8}$$

We therefore need only calculate the four spatial sectors for the one-body density matrix. The simplified form of the slater determinant for two particles in a harmonic oscillator is

$$\varphi_F(x_1, x_2) = \frac{1}{\sqrt{\pi}} e^{-\frac{1}{2}(x_1^2 + x_2^2)}(x_2 - x_1) \tag{9}$$

And so for each spatial sector of the one-body density matrix we have

$$\begin{aligned}
\rho_{1,1}(x, x') &= \frac{1}{\pi} \int dx_2 e^{-\frac{1}{2}(x'^2 + x^2)} e^{-x_2^2} (x_2 - x)(x_2 - x')\theta(x_2 - x)\theta(x_2 - x) \\
\rho_{1,2}(x, x') &= \frac{1}{\pi} \int dx_2 e^{-\frac{1}{2}(x'^2 + x^2)} e^{-x_2^2} (x_2 - x)(x' - x_2)\theta(x_2 - x)\theta(x' - x_2) \\
\rho_{2,1}(x, x') &= \frac{1}{\pi} \int dx_2 e^{-\frac{1}{2}(x'^2 + x^2)} e^{-x_2^2} (x - x_2)(x_2 - x')\theta(x - x_2)\theta(x_2 - x') \\
\rho_{2,2}(x, x') &= \frac{1}{\pi} \int dx_2 e^{-\frac{1}{2}(x'^2 + x^2)} e^{-x_2^2} (x_2 - x)(x_2 - x')\theta(x - x_2)\theta(x' - x_2)
\end{aligned}$$

These can be combined into a single simpler integral by rewriting each of them

$$\begin{aligned}
\rho_{1,1}(x, x') &= \frac{1}{\pi} \int_{\max(x,x')}^{\infty} dx_2 e^{-\frac{1}{2}(x'^2 + x^2)} e^{-x_2^2} (x_2 - x)(x_2 - x') \\
\rho_{2,2}(x, x') &= \frac{1}{\pi} \int_{-\infty}^{\min(x,x')} dx_2 e^{-\frac{1}{2}(x'^2 + x^2)} e^{-x_2^2} (x_2 - x)(x_2 - x')
\end{aligned}$$

And we can write the sum of the other two as

$$\begin{aligned}
\rho_{1,2}(x, x') + \rho_{2,1}(x, x') &= \frac{1}{\pi} \epsilon(x' - x) \int_x^{x'} dx_2 e^{-\frac{1}{2}(x'^2 + x^2)} e^{-x_2^2} (x - x_2)(x_2 - x') \\
&= \frac{1}{\pi} \int_{\min(x,x')}^{\max(x,x')} dx_2 e^{-\frac{1}{2}(x'^2 + x^2)} e^{-x_2^2} (x - x_2)(x_2 - x')
\end{aligned}$$

We can turn the sum of these terms into a single integral by noting that for each integral, the integrand is always positive, thus

$$\rho_{\uparrow,\uparrow}(x, x') = \frac{1}{\pi} \int dx_2 e^{-\frac{1}{2}(x'^2 + x^2)} e^{-x_2^2} |x_2 - x||x_2 - x'| \tag{10}$$

Which is the same one-body density matrix for two spinless, hard-core bosons. Thus we should expect results for the previous case to hold regarding the Tan Contact, the Tan Contact time dependence, and Dynamical Fermionization.

Now let's consider a slightly more interesting scenario where $|\chi\rangle = |1,0\rangle = \frac{1}{\sqrt{2}}(|\uparrow,\downarrow\rangle + |\downarrow,\uparrow\rangle)$ Using mathematica code to calculate the spin component of the one-body density matrix, we find that for any $m,n \in \{1,2\}$

$$S_{m,n}(\sigma,\sigma') = \begin{cases} \frac{1}{2} & \sigma' = \sigma = \uparrow \\ \frac{1}{2} & \sigma' = \sigma = \downarrow \\ 0 & \text{else} \end{cases} \tag{11}$$

so the simplification of the integrals will be the same as in the previous case but now there will be a constant of $\frac{1}{2}$ out front

$$\rho_{\uparrow,\uparrow}(x,x') = \rho_{\downarrow,\downarrow}(x,x') = \frac{1}{2\pi}\int dx_2 e^{-\frac{1}{2}(x'^2+x^2)} e^{-x_2^2} |x_2 - x||x_2 - x'| \tag{12}$$

For a different result, we can consider the antisymmetric singlet state $|\chi_S\rangle = |0,0\rangle = \frac{1}{\sqrt{2}}(|\uparrow,\downarrow\rangle - |\downarrow,\uparrow\rangle)$. In this case, the following gives a strongly-interacting boson wave function with this spin configuration

$$\Psi(x_1,x_2;\sigma_1,\sigma_2) = \varphi_F(x_1,x_2)\chi_S(\sigma_1,\sigma_2) \tag{13}$$

If we recall from the spinless hard-core boson case, the Bose-Fermi mapping [2] worked because the mapping function $A(x_1,\ldots,x_N)$ turned the fermion wave function Ψ_F into a wave function that 1) satsified the same Hamiltonian, 2) satsified continuity conditions, 3) satisfied same boundary conditions as Ψ_F (for HCB, Ψ must go to zero when two particles occupy the same position), and 4) satisfied boson exchange statistics (i.e., symmetry under particle exchange). When all these conditions are satisfied, the result must be a hard-core boson solution.

Similarly, for the present case, equation (13) satisfies the same conditions, where the dual antisymmetry of the spatial and spin component make the overall wave function symmetric. Because the spatial component of this wave function matches the fermion spatial component, we expect that the momentum tail for (13) will display exponential decay like fermions.

A. Non-separable Wave Function

When the spin and spatial components of the wave function are not separable like they are in the last cases,

$$\begin{aligned} \Psi(x_1,x_2;\sigma_1,\sigma_2) &= \frac{1}{\sqrt{2}}\left[\varphi_F(x_1,x_2)\chi_S(\sigma_1,\sigma_2) + \varphi_B(x_1,x_2)\chi_T(\sigma_1,\sigma_2)\right] \\ |\chi_S\rangle &= \frac{1}{\sqrt{2}}(|\uparrow,\downarrow\rangle - |\downarrow,\uparrow\rangle) \\ |\chi_T\rangle &= \frac{1}{\sqrt{2}}(|\uparrow,\downarrow\rangle + |\downarrow,\uparrow\rangle) \end{aligned} \tag{14}$$

where $\varphi_B = |\varphi_F|$, we can calculate directly from

$$\rho_{\sigma,\sigma'}(x,x') = \sum_{\sigma_2,\ldots,\sigma_N}\int dx_2\cdots dx_N \Psi^*(x,x_2,\ldots,x_N;\sigma,\sigma_2,\ldots,\sigma_N)\Psi(x',x_2,\ldots,x_N;\sigma',\sigma_2,\ldots,\sigma_N)$$

that the Tan contact will ultimately still be the same.

$$\begin{aligned} \rho_{\sigma,\sigma'}(x,x') &= \frac{1}{2}\sum_{\sigma_2}\int dx_2 \left[\varphi_F\chi_S + \varphi_B\chi_T\right]\left[\varphi'_F\chi'_S + \varphi'_B\chi'_T\right] \\ &= \frac{1}{2}\sum_{\sigma_2}\int dx_2 \varphi_B\varphi'_B\chi_T\chi'_T + \varphi_B\varphi'_F\chi_T\chi'_S + \varphi_F\varphi'_B\chi_S\chi'_T + \varphi_F\varphi'_F\chi_S\chi'_S \end{aligned} \tag{15}$$

Each spin combination can be simplified greatly

$$S_1(\sigma,\sigma') \equiv \sum_{\sigma_2} \chi_T(\sigma,\sigma_2)\chi_T(\sigma',\sigma_2) = \sum_{\sigma_2} \chi_S(\sigma,\sigma_2)\chi_S(\sigma',\sigma_2)$$
$$S_2(\sigma,\sigma') \equiv \sum_{\sigma_2} \chi_T(\sigma,\sigma_2)\chi_S(\sigma',\sigma_2) = \sum_{\sigma_2} \chi_S(\sigma,\sigma_2)\chi_T(\sigma',\sigma_2)$$
$$S_1(\sigma,\sigma') = \begin{cases} \frac{1}{2} & \sigma' = \sigma = \uparrow \\ \frac{1}{2} & \sigma' = \sigma = \downarrow \\ 0 & \text{else} \end{cases}$$
$$S_2(\sigma,\sigma') = \begin{cases} \frac{1}{2} & \sigma' = \sigma = \uparrow \\ -\frac{1}{2} & \sigma' = \sigma = \downarrow \\ 0 & \text{else} \end{cases}$$

For each of the four spatial terms in the OBDM ($\varphi_B\varphi'_B$, $\varphi_B\varphi'_F$, ...), they will have their own separate contribution to the momentum distribution. The first term will give the normal p^{-4} dependence we saw previously. The last term will decay exponentially because it is just the fermi distribution, and the second and third term will also decay exponentially

$$\begin{aligned}\int dxdx'dx_2 e^{-ip(x'-x)}\varphi_B(x,x_2)\varphi_F(x',x_2) &= \frac{1}{\pi^2}\int dx \int dx' \int dx_2 e^{-ip(x'-x)} e^{-\frac{1}{2}(x^2+x'^2)} e^{-x_2^2}|x_2-x|(x_2-x') \\ &= \frac{1}{\pi^2}\int dx_2 e^{-x_2^2}\int dx' e^{-ipx'} e^{-x'^2/2}(x_2-x')\int dx e^{ipx} e^{-x^2/2}|x_2-x| \\ \lim_{p\to\infty}\int dx e^{ipx} e^{-x^2/2}|x_2-x| &= \frac{-2e^{-\frac{1}{2}x_2^2}}{p^2} \\ \int dx' e^{-ipx'} e^{-x'^2/2}(x_2-x') &= \sqrt{2\pi} e^{-p^2/2}(x_2+ip)\end{aligned}$$

Because the integral with respect to x' decays exponentially with respect to momentum, the term as a whole for $\varphi_B(x,x_2)\varphi_F(x',x_2)$ will not contribute to the Tan contact. The Tan contact will still, therefore, be the same as the spinless case, because the only term that contributes has the same spatial component as spinless HCB. Thus

$$\lim_{p\to\infty} n_\sigma(p) = \frac{1}{2}\left(\frac{2}{\pi}\sqrt{\frac{2}{\pi}}\frac{1}{p^4}\right) S_1(\sigma,\sigma) \tag{16}$$

B. Real Space Density Profile

We will also calculate the time evolution of the momentum distribution after the trap has been turned off, but first lets calculate some other physical characteristics so that we will have something to compare the long-term behavior to. We first calculate the number density in position space

$$\begin{aligned} n_\sigma(x) &= N\rho_{\sigma,\sigma}(x,x) \\ &= \sum_{\sigma_2}\int dx_2 \varphi_B\varphi_B\chi_T\chi_T + \varphi_B\varphi_F\chi_T\chi_S + \varphi_F\varphi_B\chi_S\chi_T + \varphi_F\varphi_F\chi_S\chi_S \end{aligned} \tag{17}$$

where our particle number N is 2, thus eliminating $\frac{1}{2}$. In position space, the boson and fermion solution are the same, so

$$\begin{aligned} n_\sigma(x) &= \frac{1}{2}S_1(\sigma,\sigma)(n_F(x)+n_B(x)) + 2S_2(\sigma,\sigma)\int dx_2\varphi_F(x,x_2)\varphi_B(x,x_2) \\ &= S_1(\sigma,\sigma)n_F(x) + S_2(\sigma,\sigma)\frac{2}{\pi}\int dx_2 e^{-(x^2+x_2^2)}(x_2-x)|x_2-x| \\ &= S_1(\sigma,\sigma)n_F(x) + S_2(\sigma,\sigma)n_C(x) \end{aligned} \tag{18}$$

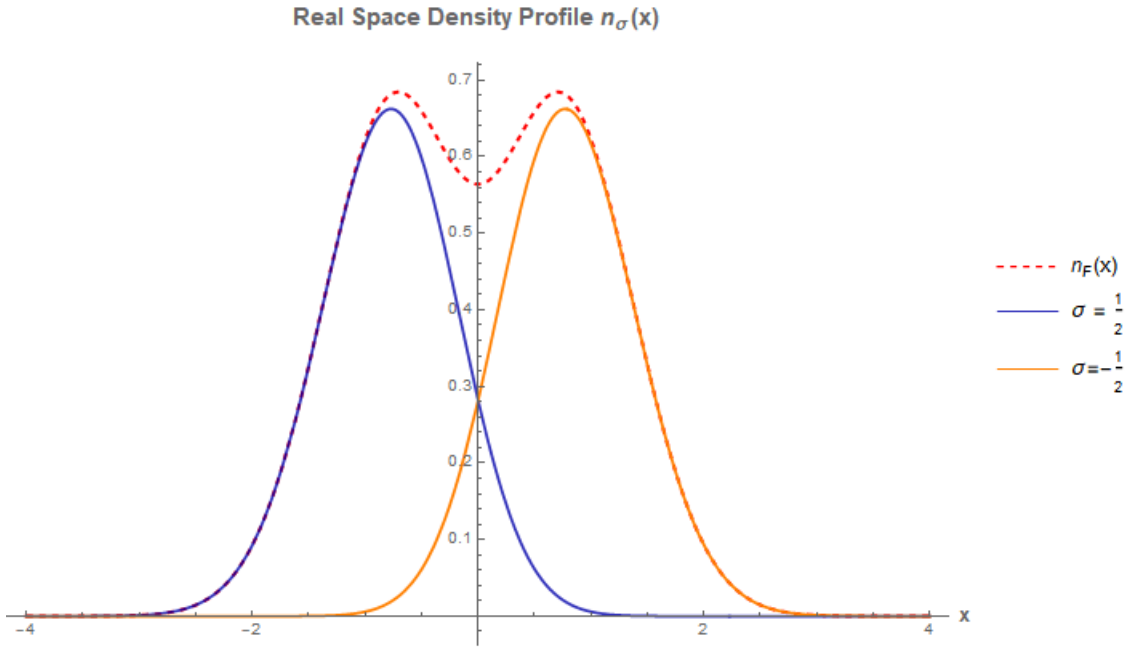

FIG. 1: We plot the real space density profile for each value of spin

where $n_F(x)$ is the real space density for two spinless fermions and $n_C(x)$ is the real density profile from the bose-fermi coupled terms in the OBDM

$$n_F(x) = \frac{e^{-x^2}(1+2x^2)}{\sqrt{\pi}} \tag{19}$$

$$n_C(x) = 2\int dx_2 \varphi_F(x,x_2)\varphi_B(x,x_2) = \frac{-2xe^{-2x^2} - e^{-x^2}(1+2x^2)\,\mathrm{erf}(x)}{\pi} \tag{20}$$

If we plot this distribution for each value of spin σ, we obtain fig. 1

C. Momentum Space Density Profile

Now we consider the density profile in momentum space before the trap has been turned off. We start with the general expression for two particles

$$n_\sigma(p) = \frac{1}{\pi}\int dx \int dx' e^{ip(x-x')}\rho_\sigma(x,x') \tag{21}$$

Plugging in our result from equation (15) and simplifying some, we can express our spin OBDM as

$$\rho_{\sigma,\sigma'}(x,x') = \frac{1}{2}S_1(\sigma,\sigma')(\rho_B(x,x') + \rho_F(x,x')) + \frac{1}{2}S_2(\sigma,\sigma')(\int dx_2 \varphi_F(x,x_2)\varphi_B(x',x_2) + \varphi_F(x',x_2)\varphi_B(x,x_2)) \tag{22}$$

We are familiar with the first two components and have calculated the momentum distribution from the boson and fermion OBDM before, thus we need only worry about the latter term. We can define our coupled term momentum space density profile as

$$n_C(p) = \frac{1}{2}\frac{N}{2\pi}\int dx_2 \int dx \int dx' e^{ip(x-x')}(\varphi_F(x,x_2)\varphi_B(x',x_2) + \varphi_F(x',x_2)\varphi_B(x,x_2)) \tag{23}$$

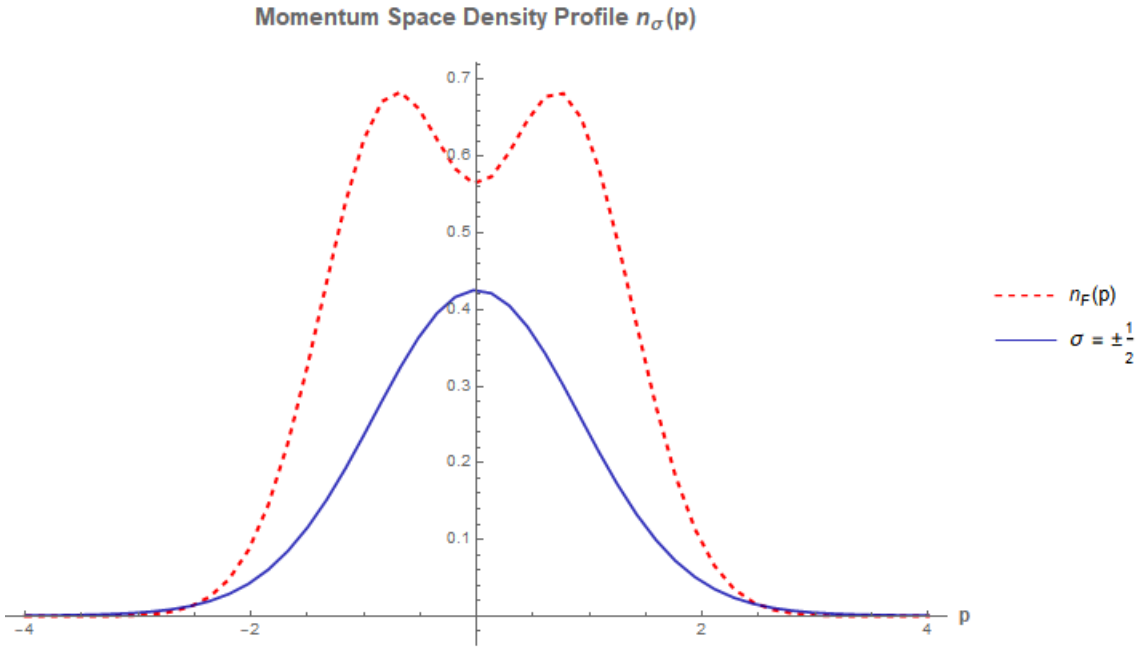

FIG. 2: Plot of momentum space density profile for (14)

It can be shown that this function will be identically zero using a parity argument as follows

$$\begin{aligned} n_C(p) &= \frac{1}{\pi}\int dx_2 \int dx \int dx' \cos(p(x-x'))\varphi_F(x,x_2)\varphi_B(x',x_2) \\ &= \frac{1}{\pi^2}\int dx_2 \int dx \int dx' \cos(p(x-x'))e^{-\frac{1}{2}(x^2+x'^2)}e^{-x_2^2}(x_2-x)|x_2-x'| \\ &= \frac{1}{\pi^2}\int dx \int dx' \cos(p(x-x'))e^{-\frac{1}{2}(x^2+x'^2)}(-2xe^{-\frac{1}{2}x^2-\frac{3}{2}x'^2} - e^{-\frac{1}{2}(x^2+x'^2)}\sqrt{\pi}(1+2xx')\,\mathrm{erf}(x')) \end{aligned}$$

Note that in the last expression the entire integrand picks up a negative sign under the transformation $x \to -x$ and $x' \to -x'$, so we should expect the integral over a symmetric region to be zero. Thus, the momentum space density profile simplifies to

$$n_\sigma(p) = \frac{1}{2}S_1(\sigma,\sigma)(n_B(p)+n_F(p)) \tag{24}$$

a plot of this distribution is given in figure 2.

D. Time Evolution of Density Profiles

Now we turn to the long term dynamics of the momentum space density profile after the trapping potential has been turned off. To find the time evolution of this system, we use a scaling transformation [6]. Our two particle OBDM will evolve as

$$\rho_{\sigma,\sigma'}(x,x';t) = \frac{1}{2b}e^{\frac{ib}{2b}(x'^2-x^2)}\left(\left(\rho_B\left(\frac{x}{b},\frac{x'}{b};0\right)+\rho_F\left(\frac{x}{b},\frac{x'}{b};0\right)\right)S_1 + \left(\rho_C\left(\frac{x}{b},\frac{x'}{b};0\right)+x\leftrightarrow x'\right)S_2\right) \tag{25}$$

where our scaling function $b(t) = \sqrt{1+t^2}$ and

$$\rho_C(x,x';0) \equiv \int dx_2 \varphi_F(x,x_2)\varphi_B(x',x_2)$$

and the momentum space density profile is

$$n_\sigma(p;t) = \frac{1}{\pi}\int dx \int dx' e^{ip(x-x')}\rho_\sigma(x,x';t) \tag{26}$$

Because our OBDM can be separated into OBDM for other systems we have already studied, our expression for the momentum space density profile can be decomposed as follows

$$n_\sigma(p;t) = \frac{1}{2}\left(n_B(p;t) + n_F(p;t)\right) S_1 + n_C(p;t) S_2 \tag{27}$$

where

$$n_C(p;t) \equiv \frac{1}{2\pi b}\int dx \int dx' e^{ip(x-x')} e^{\frac{i\dot{b}}{2b}(x'^2-x^2)} \left(\rho_C\left(\frac{x}{b},\frac{x'}{b};0\right) + x \leftrightarrow x'\right) \tag{28}$$

Switching the integration labels around, we can simplify this integral to find that

$$n_C(p;t) \equiv \frac{1}{\pi b}\int dx \int dx' \cos\left(p(x-x') + \frac{\dot{b}}{2b}(x'^2 - x^2)\right)\rho_C\left(\frac{x}{b},\frac{x'}{b};0\right) \tag{29}$$

Notice that under the transformation $x \to -x$ and $x' \to -x'$, the integrand does not change sign due to the $(x'^2 - x^2)$ term. The integrand is no longer odd, so we cannot use a parity argument like we did in equation (23) to show the integral vanishes. In fact, the integral will be non-zero.

Separating the momentum density profiles in equation (27) makes it easier to find the $t \to \infty$ behavior because it has already been shown [3] that

$$\lim_{t\to\infty} n_B(p;t) = n_F(p) = \frac{e^{-p^2}(1+2p^2)}{\sqrt{\pi}} \tag{30}$$

and the fermi distribution does not change when the trap is turned off. Thus, we only need to find the large t behavior of $n_C(p;t)$. We can simplify the expression for $n_C(p;t)$ to obtain

$$\begin{aligned}\frac{1}{2\pi b}\int dx \int dx' e^{ip(x-x')} e^{\frac{i\dot{b}}{2b}(x'^2-x^2)}\rho_C\left(\frac{x}{b},\frac{x'}{b};0\right) &= \frac{b}{2\pi}\int dx_2 \int dx \int dx' e^{ibp(x-x')} e^{\frac{i\dot{b}b}{2}(x'^2-x^2)}\varphi_F(x,x_2)\varphi_B(x',x_2) \\ &= \frac{b}{2\pi^2}\int dx_2 \int dx \int dx' e^{ibp(x-x')} e^{\frac{i\dot{b}b}{2}(x'^2-x^2)} e^{-\frac{1}{2}(x^2+x'^2)} e^{-x_2^2}(x_2 - x)|x_2 - x'|\end{aligned}$$

Then, using the stationary phase approximation we find that

$$\lim_{t\to\infty} n_C(p;t) = \frac{-2pe^{-2p^2} - e^{-p^2}(1+2p^2)\sqrt{\pi}\,\mathrm{erf}(p)}{\pi} \tag{31}$$

which is the same function as the real space density profile from equation (20). In conclusion, the large t behavior is therefore

$$\lim_{t\to\infty} n_\sigma(p;t) = S_1(\sigma,\sigma) n_F(p) + S_2(\sigma,\sigma)\frac{-2pe^{-2p^2} - e^{-p^2}(1+2p^2)\sqrt{\pi}\,\mathrm{erf}(p)}{\pi} \tag{32}$$

This result has been plotted in figure 3, thus obtaining the same profile as we observed in the real space density profile prior to expansion. Additionally, in figure 5 we plot the time evolution of $n_C(p;t)$ during this dynamical fermionization process.

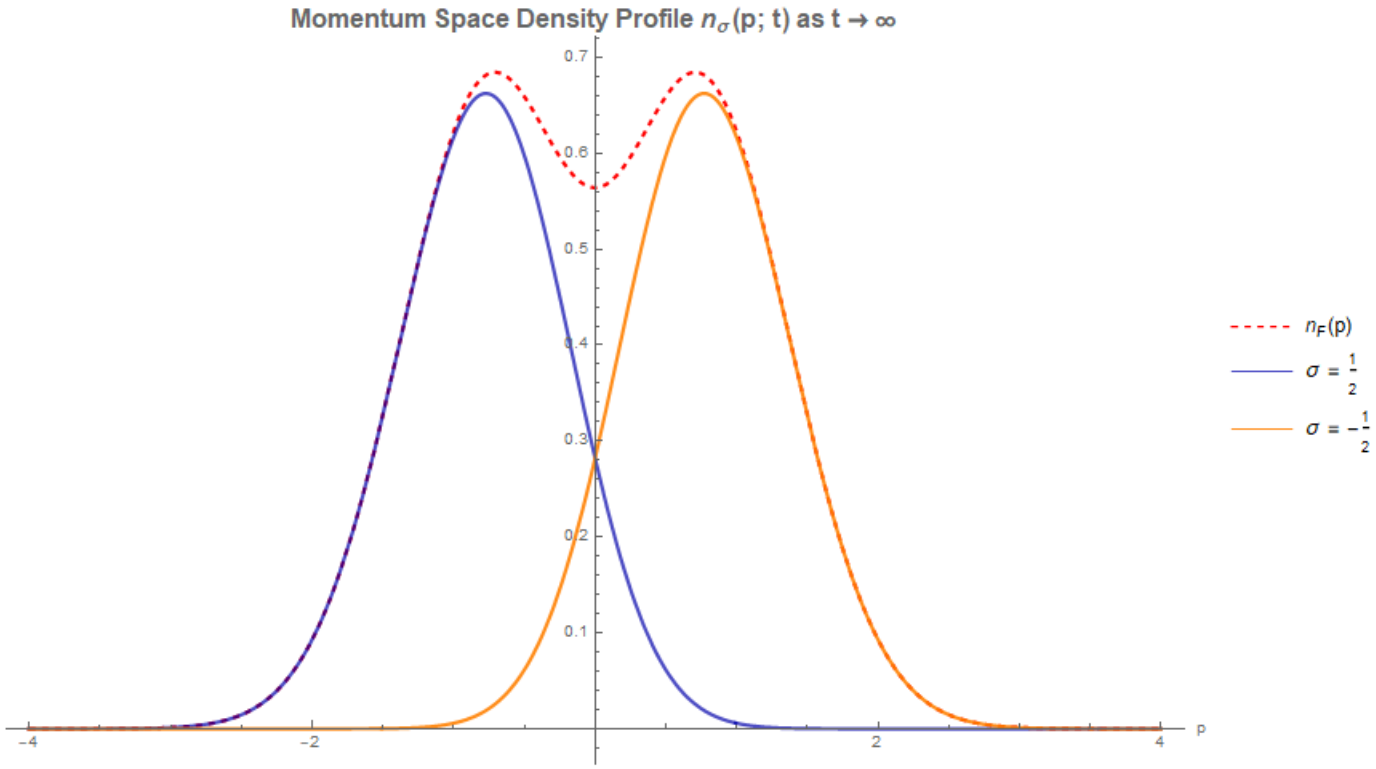

FIG. 3: Here is a plot of the momentum space density profile after the trap has been turned off and $t \to \infty$

Notice that after the trapping potential has been turned off, the $\sigma = \frac{1}{2}$ particle has a predominantly negative momentum, whereas the $\sigma = -\frac{1}{2}$ particle tends to have a positive momentum. If this is the case, we should expect to see in the RSDP for both these particles that the $\sigma = \frac{1}{2}$ particle moves to the left and the $\sigma = -\frac{1}{2}$ moves to the right. Let's calculate this to check our result.

The time dependent RSDP is given by

$$n_\sigma(x;t) = N\rho_{\sigma,\sigma}(x,x;t) \tag{33}$$

and using equation (25), we obtain the expression

$$n_\sigma(x;t) = \frac{1}{b}\left(S_1 n_F\left(\frac{x}{b};0\right) + S_2 n_C\left(\frac{x}{b};0\right)\right) \tag{34}$$

and these two functions are given analytically in equations (19) and (20) respectively. We have created an animation of the time evolution of this RSDP.

This animation confirms that the two particles will move away from each other. We can plot the location of the two modes in the RSDP (one mode for the density profile of each σ) as a function of time to illustrate this more clearly (fig. 4). As a confirmation of these results, we should see that the derivative of the position curve for each of these density peaks, should approach the final momentum of each particle after dynamical fermionization has occurred. Because the final MSDP is the same distribution as the initial RSDP however, this just means that the intial value of each density peak should approximately equal the steady state slope of each density peak trajectory.

In other words, if we denote $Q_\sigma(t)$ as the location of the RSDP mode for the particle with spin σ, then our previous analysis translates to the statement

$$Q_\sigma(0) = \lim_{t\to\infty} Q'_\sigma(t)$$

Numerical calculations confirm this with $Q_\sigma(0) \approx .771242$ and the best fit line for $Q_\sigma(t)$ in interval $t \in [100, 150]$ has slope $m = 0.771217$. This calculation is a nice indirect result of the dynamical fermionization already discussed.

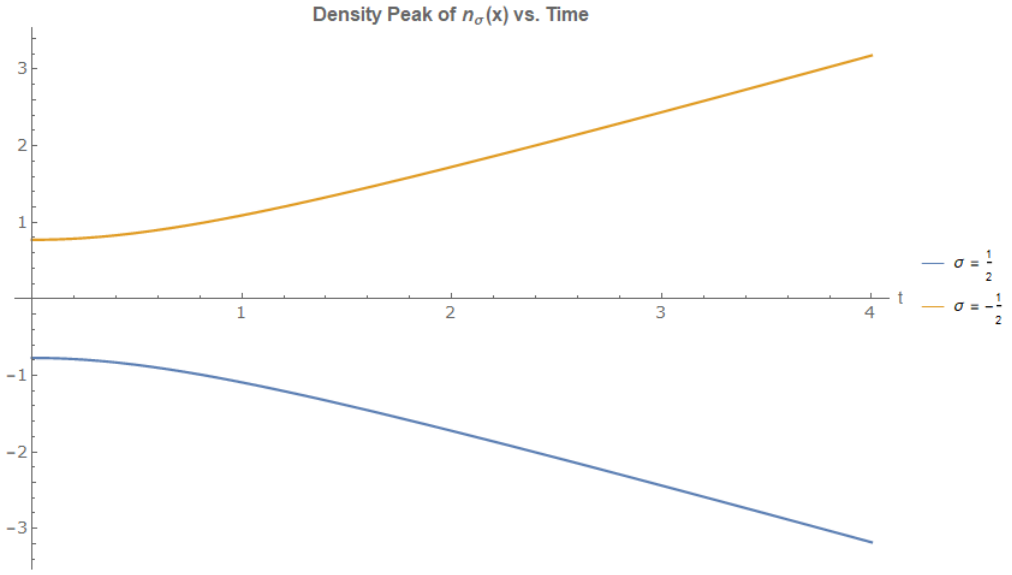

FIG. 4: This is a plot of the time evolution of the two modes in $n_\sigma(x)$ for each σ after the trapping potential has been turned off. The two peaks move away from each other and approach a constant momentum.

E. Non-separable Wave Function with Constant Phase Difference

Now we consider how the above results would change if we modified equation (14) so that the two terms differed by a constant phase, viz.

$$\Psi(x_1, x_2; \sigma_1, \sigma_2) = \frac{1}{\sqrt{2}} \left[\varphi_F(x_1, x_2)\chi_S(\sigma_1, \sigma_2) + e^{i\theta}\varphi_B(x_1, x_2)\chi_T(\sigma_1, \sigma_2)\right], \qquad \theta \in [0, 2\pi) \tag{35}$$

For the real space density profile (RSDP), we obtain a different expression from before

$$n_\sigma^\theta(x) = \frac{1}{2}S_1(\sigma, \sigma)(n_F(x) + n_B(x)) + S_2(\sigma, \sigma) \int dx_2 \left[\varphi_F(x, x_2)\varphi_B(x, x_2)e^{i\theta} + \varphi_F(x, x_2)\varphi_B(x, x_2)e^{-i\theta}\right]$$

and we can simplify this latter term

$$\begin{aligned} n_C^\theta(x) &= \int dx_2 \left[\varphi_F(x, x_2)\varphi_B(x, x_2)e^{i\theta} + \varphi_F(x, x_2)\varphi_B(x, x_2)e^{-i\theta}\right] \\ &= 2\cos(\theta) \int dx_2 \varphi_F(x, x_2)\varphi_B(x, x_2) \\ &= \frac{2\cos(\theta)}{\pi} \int dx_2 e^{-\frac{1}{2}(x^2 + x'^2)} e^{-x_2^2}(x_2 - x)|x_2 - x| \\ &= -\frac{\cos(\theta)}{\pi}(2xe^{-2x^2} + e^{-x^2}\sqrt{\pi}(1 + 2x^2)\,\mathrm{erf}(x)) \end{aligned}$$

and thus

$$n_C^\theta(x) = -\frac{\cos(\theta)}{\pi}(2xe^{-2x^2} + e^{-x^2}\sqrt{\pi}(1 + 2x^2)\,\mathrm{erf}(x)) \tag{36}$$

which is the same expression for RSDP as in equation (20), differing only by a factor of $\cos(\theta)$ in front. We conclude that the RSDP for this new wave function is

$$n_\sigma^\theta(x) = S_1(\sigma, \sigma)n_F(x) + S_2(\sigma, \sigma)n_C^\theta(x) \tag{37}$$

See this gif to observe how the θ dependence affects the RSDP. As we saw in figure 1, the RSDP for $\sigma = \frac{1}{2}$ is skewed toward negative momentum and the RSDP for $\sigma = -\frac{1}{2}$ is skewed toward positive momentum. The gif illustrates that

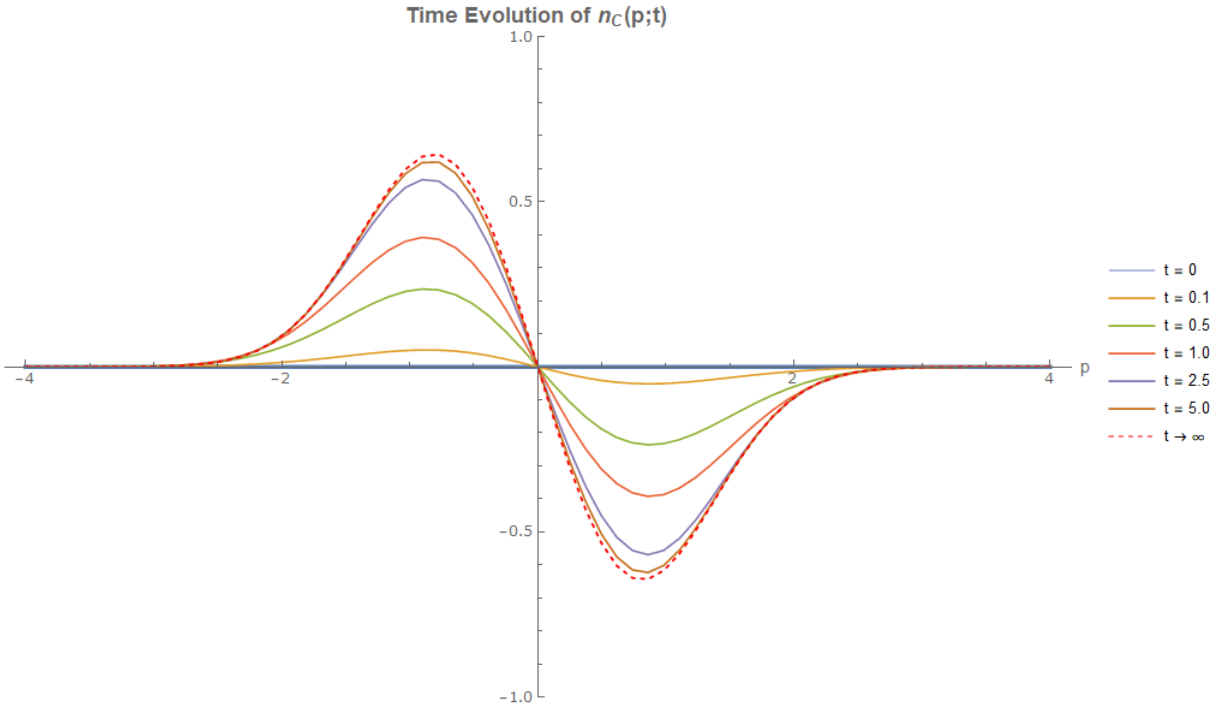

FIG. 5: Plot of the time evolution of $n_C(p;t)$. The splitting that occurs during dynamical fermionization of the momentum distribution for each value of spin σ is due to the change n_C. The red, dashed line is the asymptotic analytic expression given in equation (31). There is also an animated gif of this time evolution.

as we increase θ this trend is reversed once during $\theta \in [0, \pi]$ so that the $\sigma = \frac{1}{2}$ distribution is transformed into the $\sigma = -\frac{1}{2}$ distribution (and vice-versa) and then the trend is reversed once again while $\theta \in [\pi, 2\pi)$.

The momentum space density profile (MSDP) will also change with θ. For the entire MSDP, we obtain the expression

$$n_\sigma^\theta(p) = \frac{1}{2}\left(n_B(p) + n_F(p)\right) S_1 + n_C^\theta(p) S_2 \tag{38}$$

where $n_C^\theta(p)$ from equation (23) becomes

$$n_C^\theta(p) = \frac{1}{2}\frac{N}{2\pi}\int dx_2 \int dx \int dx' e^{ip(x-x')}(\varphi_F(x,x_2)\varphi_B(x',x_2)e^{i\theta} + \varphi_F(x',x_2)\varphi_B(x,x_2)e^{-i\theta}) \tag{39}$$

which we simplify to

$$\begin{aligned} n_C^\theta(p) &= \frac{1}{\pi^2}\int dx_2 \int dx \int dx' \cos(p(x-x')+\theta) e^{-\frac{1}{2}(x^2+x'^2)} e^{-x_2^2}(x_2 - x)|x_2 - x'| \\ &= -\frac{\sin(\theta)}{\pi^2}\int dx_2 \int dx \int dx' \sin(p(x-x')) e^{-\frac{1}{2}(x^2+x'^2)} e^{-x_2^2}(x_2 - x)|x_2 - x'| \end{aligned}$$

this integral does not have an integrand with odd parity and will have a non-zero contribution to the MSDP for $\theta \neq 0$. We have created a gif of how the momentum distribution changes with θ. When $\theta = 0$, we saw in figure 2 that the momentum distribution for each spin value was symmetric with respect to p. As θ is increased, we see in the gif that this symmetry is broken as the distribution for each spin value is shifted toward the left or the right depending on the exact value of θ and σ.

Lastly, we consider the MSDP after the trapping potential has been turned off in the $t \to \infty$ limit. In order to calculate

$$n_\sigma^\theta(p;t) = \frac{1}{2}\left(n_B(p;t) + n_F(p;t)\right) S_1 + n_C^\theta(p;t) S_2 \tag{40}$$

$$\lim_{t\to\infty} n_\sigma^\theta(p;t) = n_F(p;t) S_1 + \lim_{t\to\infty} n_C^\theta(p;t) S_2 \tag{41}$$

we must find the limit of the last term. Starting with the inital θ dependent expression

$$n_C^\theta(p;t) \equiv \frac{b}{\pi^2}\int dx \int dx' \int dx_2 \cos\left(bp(x-x') + \frac{\dot{b}b}{2}(x'^2 - x^2) + \theta\right) e^{-\frac{1}{2}(x^2+x'^2)} e^{-x_2^2}(x_2 - x)|x_2 - x'| \tag{42}$$

expanding the cosine in terms of exponentials and applying the stationary phase approximation again leaves us with the following asymptotic expression

$$\lim_{t\to\infty} n_C^\theta(p;t) = \frac{\cos(\theta)}{\pi}(-2pe^{-2p^2} - e^{-p^2}(1+2p^2)\sqrt{\pi}\,\mathrm{erf}(p)) \tag{43}$$

differing from the previous asymptotic expression when θ was excluded (31) only by a factor of $\cos(\theta)$. The θ-dependence will be the same as for the RSDP, therefore. Again, we have created a gif to animate this θ dependence.

An animation of the full time dependence for various theta can be viewed here

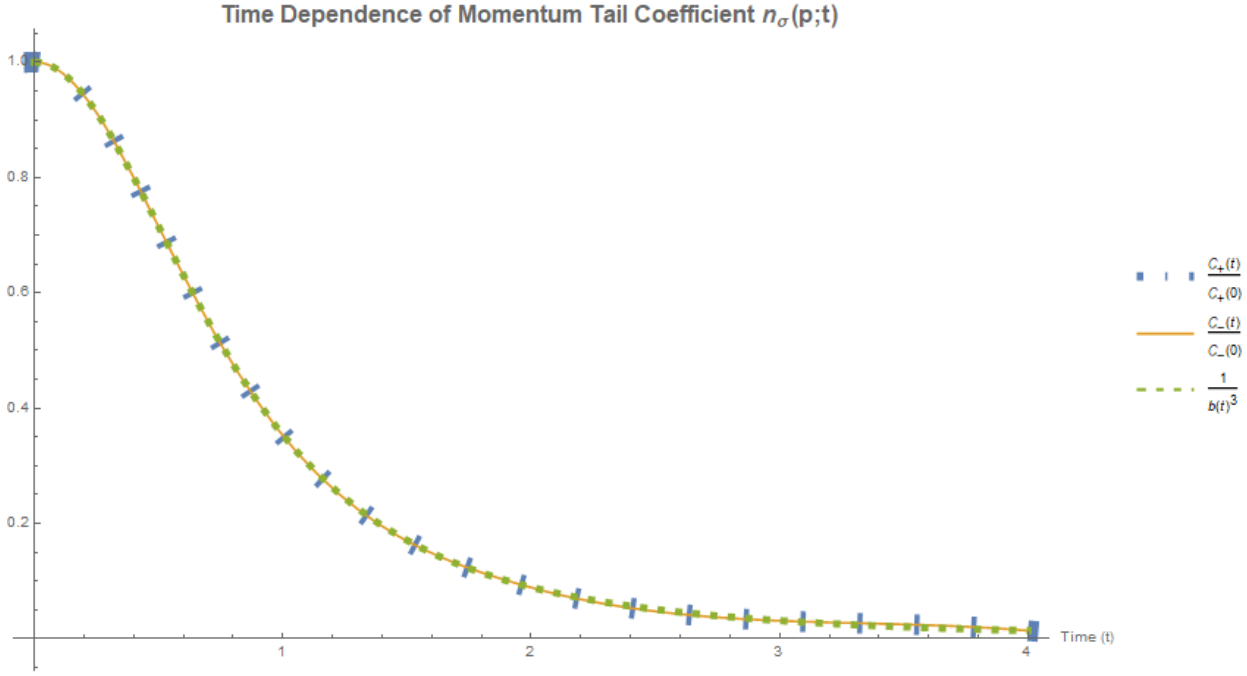

FIG. 6: This is a plot of the time dependence of the Tan Contact for $n_\sigma(p)$ with $\sigma = \frac{1}{2}$ and $\sigma = -\frac{1}{2}$. $C_+(t)$ denotes the Tan Contact for the former and $C_-(t)$ denotes the Tan Contact for the latter. To examine just the time dependent behavior, the Tan Contact function has been divided by its value at $t = 0$. The calculations required for this plot assumed that $\theta = 0$. These plots were created by numerically calculating the Tan Contact for several values of t and then interpolating intermediate points for the sake of plotting.

Inspecting equation (39) again, we see that the n_B term is the only term that contribute to the Tan Contact of n_σ because all the other terms decay exponentially with p. The time dependence of the Tan Contact, therefore, will be the same as in the spinless HCB case, differing only by a constant. We have numerically calculated and plotted this time dependence in the plot in figure 6. The plot shows that numerical calculation agrees with theoretical prediction that the Tan Contact should have a decay proportional to $\frac{1}{b(t)^3}$, where the constant is given in equation (16).

III. EFFECTS OF ANHARMONICITY ON DYNAMICAL FERMIONIZATION

Recall our previous investigation of dynamical fermionization of strongly-interacting, spinless bosons. We assumed that two spinless bosons were confined in a harmonic trap, and we calculated the long-term dynamics of the MSDP in the scenario where the trapping potential is turned off. Now we would like to consider the effects of adding anharmonicity to the Hamiltonian of this system, thus giving

$$H = \sum_{i=1}^{N}\left[-\frac{1}{2}\frac{\partial^2}{\partial x^2} + \frac{1}{2}x_i^2 + \lambda x^4\right] + g\sum_{i<j}\delta(x_i - x_j) \tag{44}$$

To find the long term dynamics of such a system, we will use the Imaginary Time Propagation method to compute the new ground state and first excited state for two fermions [1, 4]. Then, once we have these eigenstates in position space $\phi_0(x)$ and $\phi_1(x)$ we can transform them to momentum space to obtain $\widetilde{\phi_0}(p)$ and $\widetilde{\phi_1}(p)$. After obtaining the wave functions in momentum space, it is very easy to find $\phi_0(x,t)$ and $\phi_1(x,t)$ at any time t using the expression

$$\phi_i(x,t) = \int dp e^{ipx} \widetilde{\phi}_i(p) e^{-i\frac{p^2}{2}} \tag{45}$$

Once we have the time evolution of the first two fermion eigenstates, we can numerically compute the time evolution of the OBDM and density profiles using the Bose-Fermi mapping and other standard methods.

I will now describe the results I have obtained and the methods I implemented for the case where $\lambda = 0.1$.

Numerical Scheme & Instability

To implement the Imaginary Time Propagation method (ITP), I had initially used a Forward Euler method to solve the resulting PDE. This proved to be problematic, however, because when potential terms are added, the instability of this method becomes much worse. To overcome these issues, I switched to using a Backward Euler method, which is usually unconditionally stable.

Ground State & First Excited State

After using the proper numerical scheme, I used to the ITP method to obtain the ground state for the Hamiltonian

$$H = -\frac{1}{2}\frac{\partial^2}{\partial x^2} + \frac{1}{2}x^2 + \lambda x^4 \tag{46}$$

by using the harmonic trap ground state as the starting trial function. To find the the first excited state for 46, we must use a trial function that is orthogonal to the actual ground state of 46. The first excited state for the harmonic potential satisfies this constraint because it is an odd function.

Figures 7 and 8 plot the resulting ground state and first excited state. I have plotted along with each the corresponding eigenstate for a harmonic trap.

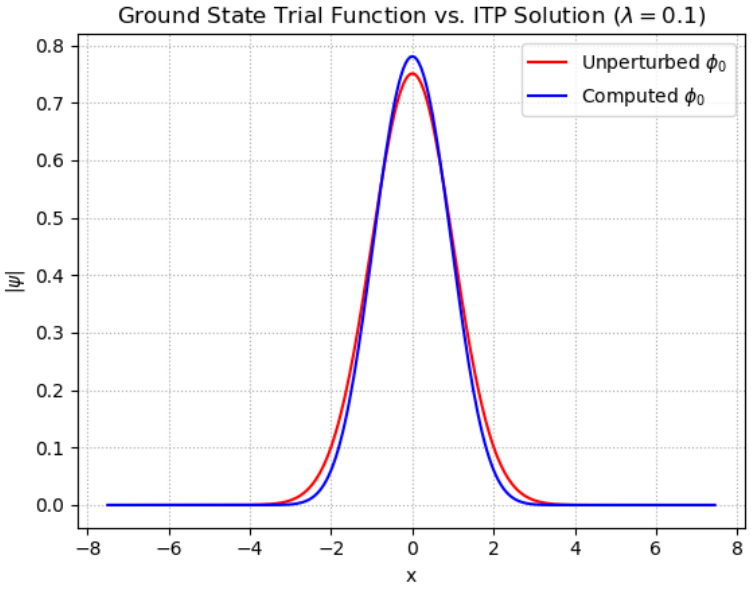

FIG. 7: Ground state wave function for anharmonic potential. Computed ϕ_0 is the anharmonic wave function "computed" from the ITP method. The red plot depicts the ground state for harmonic potential.

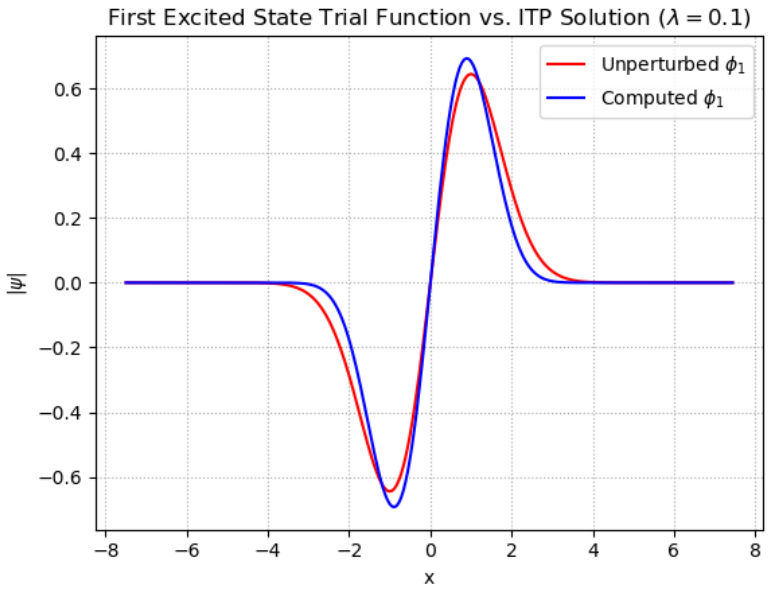

FIG. 8: First excited state for anharmonic potential. Labeling convention is same as in previous plot.

To ensure that these computed eigenstates are correct, I compute the energy of the trial wave function at each iteration to ensure that it is indeed increasing. To make the convergence easier to plot for each eigenstate, I have subtracted the final energy value from the energy value at each iteration of the trial wave function, which is why both curves appear to converge to zero in the plot. Figure 9 shows that energy converges to some value for each eigenfunction.

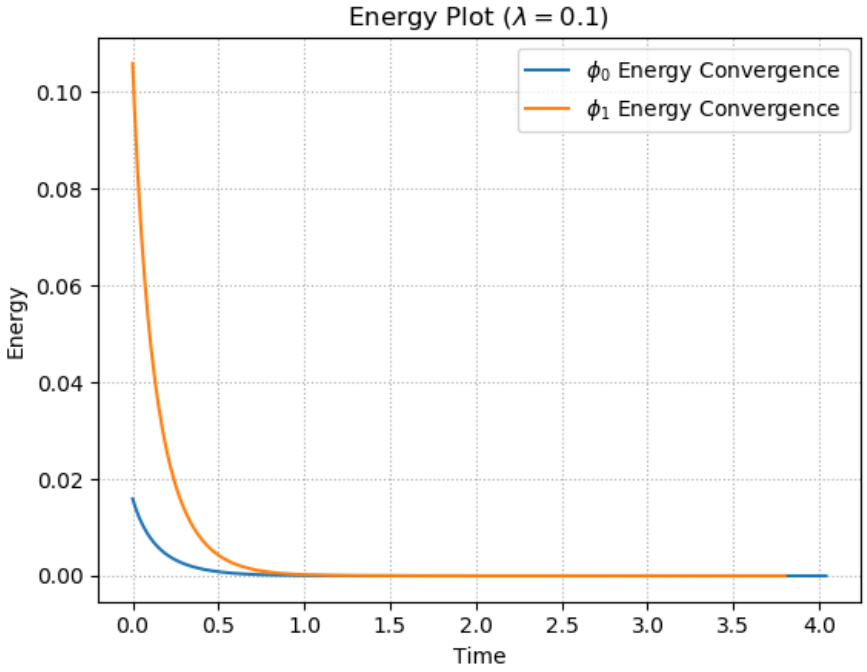

FIG. 9: At every tenth time step of my ITP method, I have recorded the energy of the trial solution. For this plot, I recorded the energy at different iterations and subtracted the final energy the method converged to. Thus, these plots merely show the relationship between the initial energy of the trial function and the energy of successive iterations.

As a check on my code, I have ensured that the eigenstates my program finds in the case where $\lambda = 0$ indeed matches the analytically known results for the eigenstates of the harmonic potential.

Momentum Distributions, OBDM, MSDP

After obtaining the eigenstates, I fourier transform these wave functions to find their representation in momentum space. I have checked that my code for the fourier transformation is correct by ensuring that its result for the harmonic eigenstates match the analytically known result. After doing so, I calculated the momentum distribution $\widetilde{\phi}_i(p)$ of each of these eigenstates and have plotted $\widetilde{\phi_0}(p)$ in figure 10.

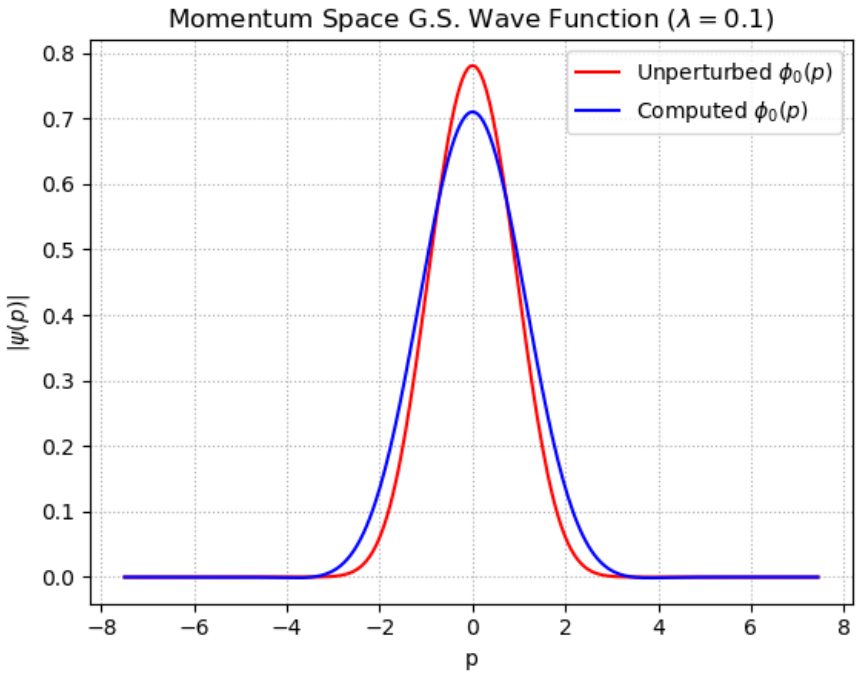

FIG. 10: Momentum distribution for ground state wave function.

By using equation 45, we can calculate the time evolution of each eigenstate in the situation where both trapping potentials are suddenly turned off. Then, $\phi_i(x,t)$ can be used to compute $\rho_B(x,x';t)$ by using the bose-fermi mapping on the slater determinant.

Again, when $\lambda = 0$, the OBDM can be calculated analytically and compared to my computed values. I did this to check my code and found that my computed OBDM for a harmonic potential differed from the exact answer by an average value of 10^{-5}. To check the validity of this time evolution method, I also made sure that the particle number of the RSDP is conserved through time, which I have plotted in figure 11

Figure 12 depicts how the RSDP is affected by the addition of the quartic potential term to the Hamiltonian. Of course, the question we are really interested in is what happens to the MSDP after all trapping potentials are turned off? Even when the quartic perturbation is added to the Hamiltonian, we still see dynamical fermionization occur. Though it is difficult to see, figure 13 shows that the MSDP at $t = 6$ (orange figure) is almost identical to the initial MSDP of non-interacting fermions in an anharmonic potential (purple).

For reference, I have also plotted other relevant Momentum Space Density Profiles that are very similar. The green figure plots the initial RSDP of the harmonically confined bosons. Because the quartic perturbation breaks the symmetry between momentum space and position space, the initial RSDP and final MSDP are different now. Nonetheless, the plot shows that as the time t increases, the bosonic MSDP asymptotically approaches the fermi MSDP

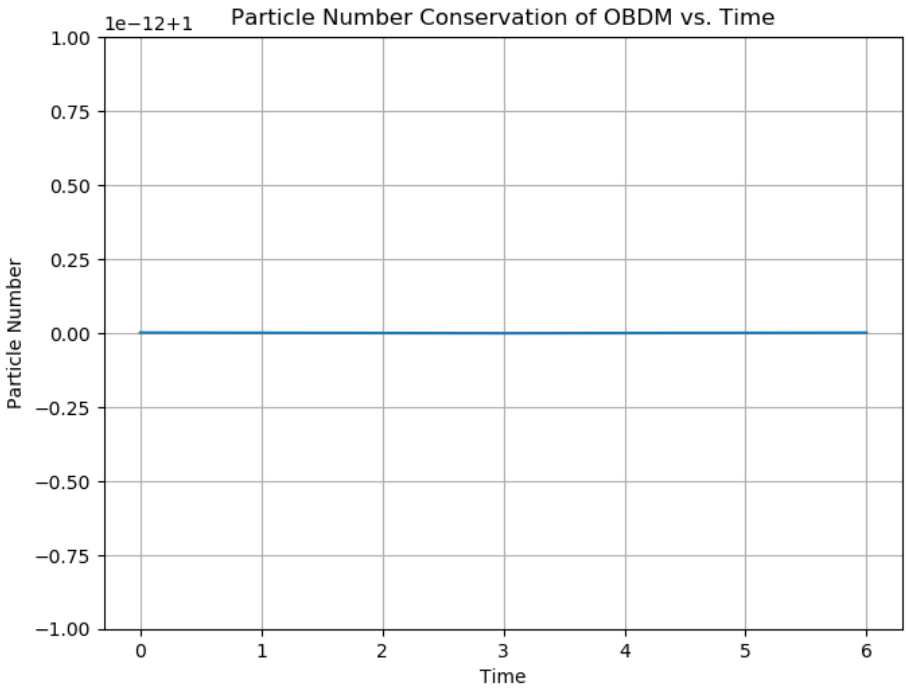

FIG. 11: This plot depicts how the particle number of the RSDP changes in time with my time evolution method. For my purposes, I only calculated the RSDP at $t = 0, 3, 6$, so this plot only has three distinct points. But we can nonetheless see that the particle number changes by less than one part in 10^{-12}.

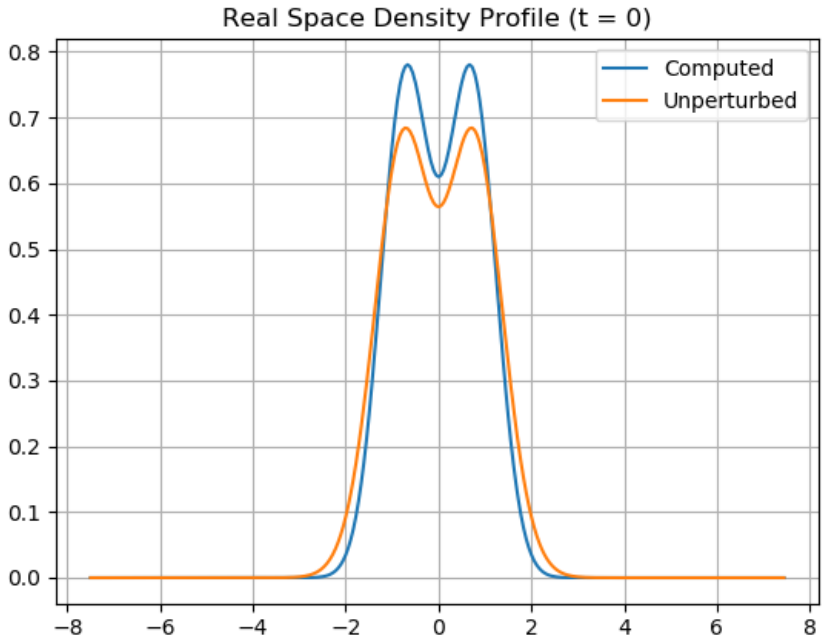

FIG. 12: This figure plots the RSDP before the trapping potential is turned off. The blue figure is the anharmonic RSDP and the orange figure is the RSDP for two harmonically confined fermions.

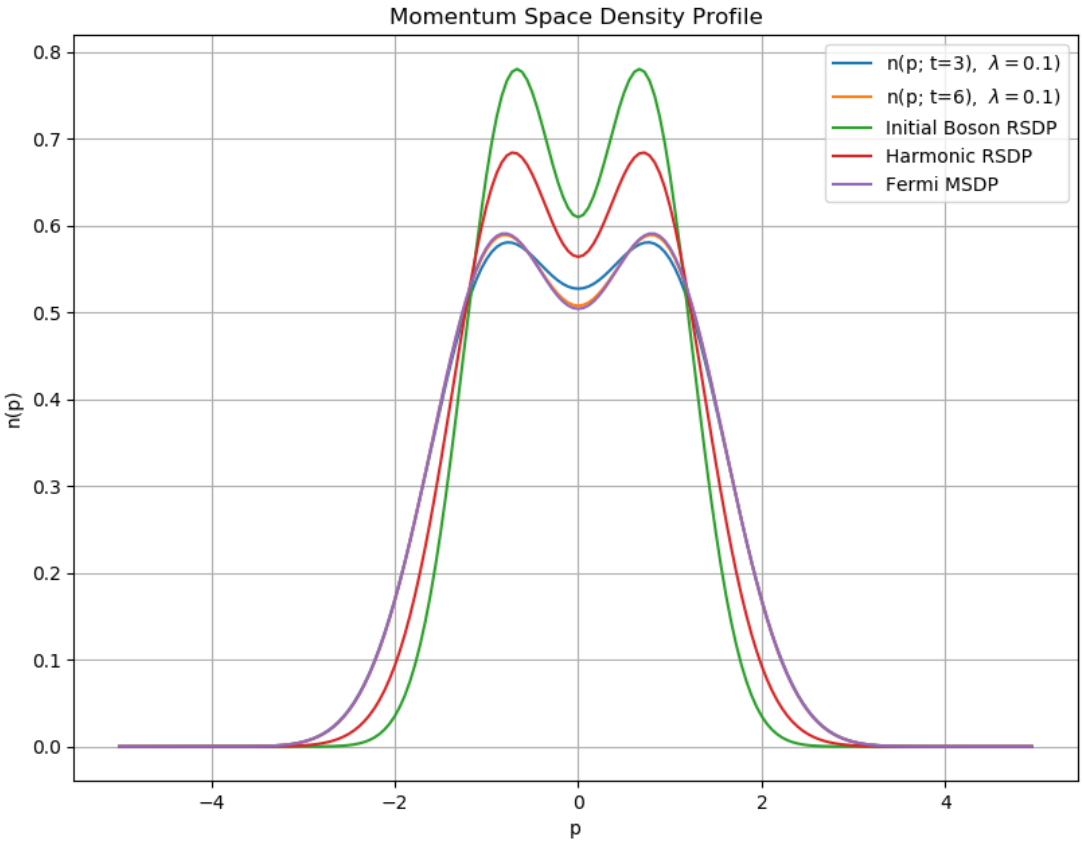

FIG. 13: This figure plots the evolution of the MSDP, given by $n(p;t)$, for the anharmonically confined bosons and compares the initial and final MSDP to other density profiles. Initial Boson RSDP is the RSDP for bosons before the trapping potential has been turned off. Harmonic RSDP is the RSDP for bosons/fermions (same in this case) with a purely harmonic trapping potential, and the Fermi MSDP is the MSDP of fermions with the anharmonic potential. We can see that with the anharmonic term, the initial RSDP is larger near the center than the initial harmonic RSDP, and, correspondingly, the final MSDP is less than the initial harmonic RSDP.

Asymmetric Anharmonicity

It is rather surprising to find that dynamical fermionization will still occur even when the bosons are not harmonically confined. But now we ask, what factor does the symmetry of the Hamiltonian play in this? Because the parity operator commutes with Hamiltonian in equation 46, the resulting eigenstates are symmetric. If we add a cubic term to this Hamiltonian to obtain

$$H = -\frac{1}{2}\frac{\partial^2}{\partial x^2} + \frac{1}{2}x^2 + \alpha x^3 + \lambda x^4 \tag{47}$$

our eigenstates will no longer be eigenstates of the parity operator, so we will have asymmetric eigenfunctions. I have conducted the same analysis to that above for this situation, where $\lambda = 0.05$ and $\alpha = 0.1$. In my results, I demonstrate that dynamical fermionization still occurs and I discuss some symmetry properties of the MSDP to understand this better.

Following the same procedure as before, the ground state and first excited state are no longer even/odd with this potential, and the initial RSDP is no longer symmetric either (figure 14)

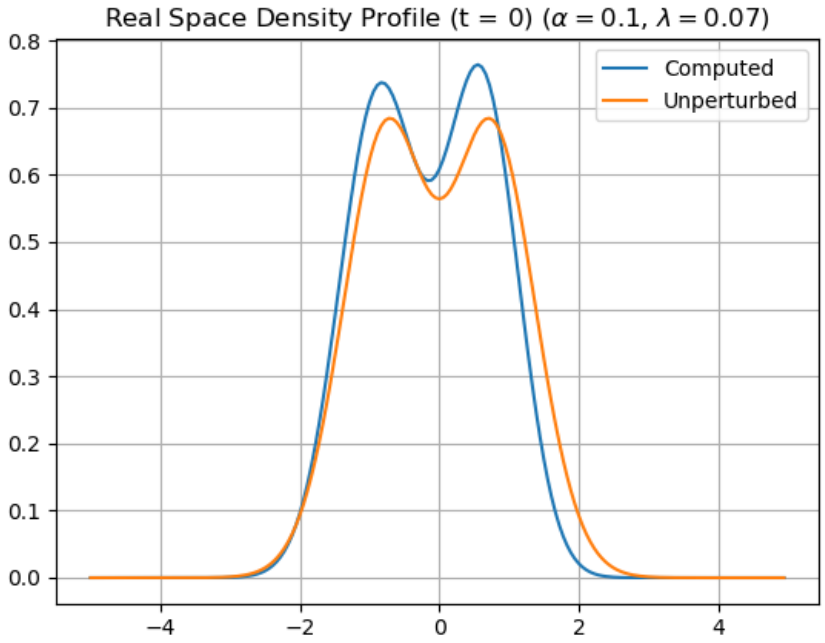

FIG. 14: This figure plots the initial real space density profile for the case of an asymmetric trapping potential

Nonetheless, the momentum space density profile remains even, and we still observe dynamical fermionization in this trapping potential.

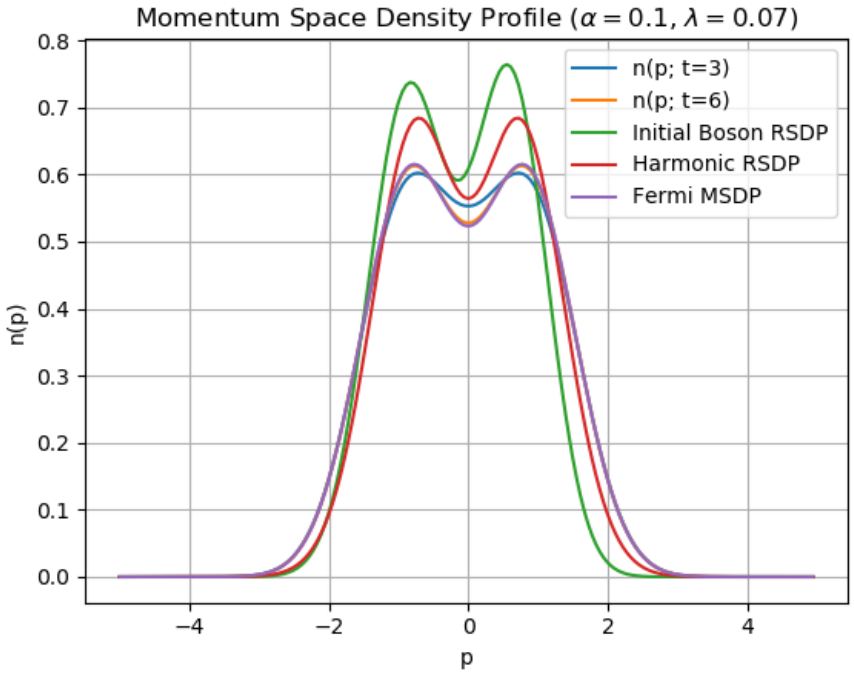

FIG. 15: This figure plots the MSDP for various situations. We can see that the final MSDP of the

Admittedly, it is rather curious to see the asymmetric RSDP juxtaposed with the completely symmetric time

evolution of the MSDP, but this can be explained. Recalling our expression for the real space density profile

$$n(x) = N\rho(x,x) = \int dx_2 \Psi^*(x,x_2)\Psi(x,x_2) \tag{48}$$

the symmetry of this expression under the exchange $x \to -x$ is completely dependent on the eigenstates of our Hamiltonian, which make up the slater determinant $\Psi(x_1,x_2)$. In general, $\Psi(x_1,x_2)$ is only symmetric under exchange $x_1 \to x_2$, which is guaranteed by our bose-fermi mapping of the slater determinant. Total wave function $\Psi(x_1,x_2)$ will have parity symmetry when the eigenstates $\phi_0(x)$ and $\phi_1(x)$ that comprise it have parity symmetry.

This symmetry came from the fact that the parity operator $\hat{\Pi}$ commuted with the Hamiltonian in equation (46), which meant that our eigenstates were degenerate in the parity subspace. Once we know this to be true, an arbitrary eigenbasis $\phi_0, \phi_1, \ldots$ for the Hamiltonian can simultaneously be eigenstates of $\hat{\Pi}$. For the purposes of this discussion, I will call this kind of symmetry *strong parity symmetry*. This means that $[H,\Pi] = 0$ and that the eigenstates of H will be even or odd. Or expressed in position space this means $\phi(-x) = \pm\phi(x)$. If the Hamiltonian in equation (47) does not have this symmetry, then why is the MSDP even? I would like to show that while strong parity symmetry is sufficient for an even MSDP, it is not necessary. First I will make some comments on the momentum space density profile and proceed to a more formal justification of this claim.

For two particles, the momentum space density profile is

$$n(p;t) = \frac{N}{2\pi}\int dx \int dx' e^{ip(x-x')}\rho(x,x';t) \tag{49}$$

The integration variables are arbitrary, so we can change them without affecting the value of the expression.

$$\begin{aligned}
n(p;t) &= \frac{1}{2}\frac{N}{2\pi}\left(\int dx \int dx' e^{ip(x-x')}\rho(x,x';t) + \int dx' \int dx e^{ip(x'-x)}\rho(x',x;t)\right) \\
&= \frac{1}{2}\frac{N}{2\pi}\left(\int dx \int dx' e^{ip(x-x')}\rho(x,x';t) + \int dx' \int dx e^{-ip(x-x')}\rho(x,x';t)^*\right) \\
&= \frac{1}{2}\frac{N}{2\pi}\int dx \int dx' \left(e^{ip(x-x')}\rho(x,x';t) + e^{-ip(x-x')}\rho(x,x';t)^*\right) \\
&= \frac{1}{2}\frac{N}{2\pi}\int dx \int dx' \,\mathrm{Re}\left[e^{ip(x-x')}\rho(x,x';t)\right]
\end{aligned}$$

This follows directly from the definition of the one-body density matrix that satisfies $\rho(x,x') = \rho(x',x)^*$. We conclude

Remark 1. *The momentum space density profile $n(p;t)$ for any configuration of spinless particles will be real.*

In the case where ρ is real, the integrand can be simplified to be

$$n(p;t) = \frac{1}{2}\frac{N}{2\pi}\int dx \int dx' \cos(p(x-x'))\rho(x,x';t) \tag{50}$$

from which it is apparent that $n(p)$ will be even. Now, for all the cases we have considered, the one body density matrix at $t = 0$ is real because it is composed of eigenfunctions that are solutions to a real differential equation given by the time-independent Schrodinger equation. If $\rho(x,x';t)$ is the OBDM for a system of particles after a trapping potential has been turned off, $\rho(x,x';t)$ will in general not be strictly real for $t > 0$.

[1] M. L. Chiofalo, S. Succi, and M. Tosi. Ground state of trapped interacting bose-einstein condensates by an explicit imaginary-time algorithm. *Physical Review E*, 62(5):7438, 2000.
[2] M. Girardeau. Relationship between systems of impenetrable bosons and fermions in one dimension. *Journal of Mathematical Physics*, 1(6):516–523, 1960.
[3] A. Minguzzi and D. Gangardt. Exact coherent states of a harmonically confined tonks-girardeau gas. *Physical review letters*, 94(24):240404, 2005.
[4] P. Muruganandam and S. K. Adhikari. Fortran programs for the time-dependent gross–pitaevskii equation in a fully anisotropic trap. *Computer Physics Communications*, 180(10):1888–1912, 2009.
[5] L. Yang, L. Guan, and H. Pu. Strongly interacting quantum gases in one-dimensional traps. *Physical Review A*, 91(4):043634, 2015.
[6] Y. B. Zel'dovich et al. *Quantum mechanics: selected topics*. World Scientific, 1998.